



# Automated mapping of conformity between topographic and geological surfaces

Ross K. Meentemeyer\*, Aaron Moody

*Department of Geography, University of North Carolina at Chapel Hill, 203 Saunders Hall, Chapel Hill, NC 27599-3220, USA*

Received 30 June 1999; received in revised form 23 December 1999; accepted 23 December 1999

---

## Abstract

We present a technique to produce spatially distributed fields of geometric alignment between topography and the orientation of geologic bedding planes (topographic/bedding-plane intersection angle). Computation and digital mapping of the topographic/bedding-plane intersection angle (TOBIA) requires the derivation of four spatially distributed variables: topographic slope, slope aspect, bedding dip, and dip azimuth. Slope and slope aspect surfaces are derived from a high resolution (10 m) digital elevation model. Ordinary kriging is used to interpolate spatially continuous fields of dip azimuth and dip from point measurements of strike and dip. Using these variables, TOBIA can be mapped either categorically as slope types, or as a continuous index. Categorical mapping requires two steps. First, slopes are classified into three functional types based on the alignment between the dip azimuth and slope aspect. Slopes are then further partitioned based on the alignment between slope angle and dip angle. Continuous computations of TOBIA rely on a geometric equation using all four variables. The methods provide an efficient means for estimating topographic/bedding plane intersection angles over large areas. Resulting surfaces are useful for a variety of landscape-scale modeling applications, such as the prediction of potential hillslope failure, hydrologic flow paths, and vegetation patterns. © 2000 Elsevier Science Ltd. All rights reserved.

*Keywords:* Bedding planes; Strike and dip; Topography; DEM; Digital terrain analysis

---

## 1. Introduction

We present a set of computational techniques to compute and digitally map the orientation of topographic slope and aspect relative to the strike and dip of bedding planes in a spatially distributed framework. Typically, this relationship (the topographic/bedding-plane intersection angle) is known only at point locations where strike and dip have been determined in

the field. Although this relationship has been mapped (e.g. Eaton, 1986), it has proven so tedious to do so that studies requiring such data are limited to specific slopes or theoretical scenarios (e.g. Freeze and Cherry, 1979; Selby, 1993). The availability of digital elevation models (DEMs) and methods for digital terrain analysis creates an opportunity to characterize these relationships over much larger areas using geologic structure data in combination with DEMs in a spatially distributed framework. DEMs have been used alone (e.g. Chorowicz et al., 1991; Ichoku et al., 1994) and in combination with satellite imagery (e.g. Morris, 1991; Chorowicz et al., 1995) to estimate the strike and dip of bedding planes. Little work exists, however, on

---

\* Corresponding author. Tel.: +1-919-962-5303; fax: +1-919-962-1537.

*E-mail address:* rkm@email.unc.edu (R.K. Meentemeyer).

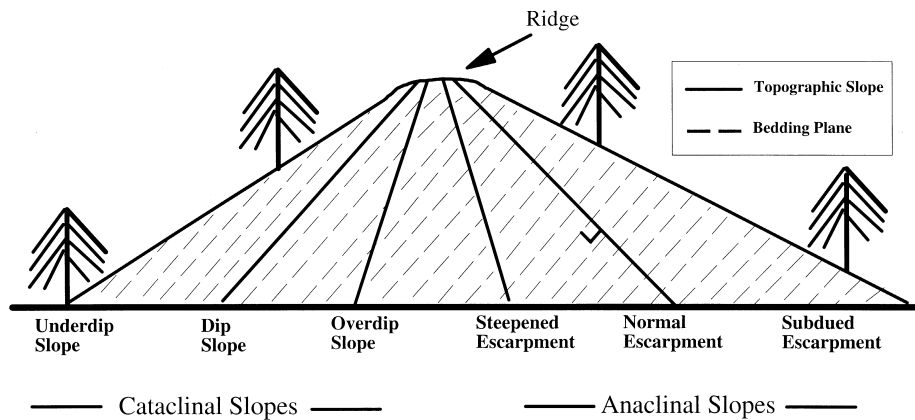


Fig. 1. Classification of alignment between topography and bedding planes. Orthoclinal orientation is not shown.

producing spatially distributed fields that represent the degree of conformity between topographic and geological surfaces.

Geometric relationships between topography and geologic structure can influence sub-surface drainage and mass wasting (Freeze and Cherry, 1979; Selby, 1993). This is particularly evident where geologic structure is characterized by penetrative discontinuities, such as sedimentary bedding or schistosity (Sander, 1970; Cruden, 1989). As such, the degree of conformity between topographic slope and aspect relative to the strike and dip of bedding planes is often measured in these contexts (e.g. Cruden and Hu, 1996).

When a rock mass contains a distinct bedding plane, TOBIA can be categorized into three basic classes (Fig. 1) (Cruden, Hu, 1996; Cruden, 1988, 1989; Powell, 1875). If the bedding plane dips in the same direction as the slope, the slope is classified as **cataclinal**. If the bed dips in the direction opposite to the slope, then the slope is classified as **anaclinal**. Cases where the azimuth of the dip direction is perpendicular to the azimuth of the slope direction are referred to as **orthoclinal** slopes (not shown in Fig. 1). Cataclinal and anacinal slopes may be further divided based on the alignment between the dip of the bedding plane and topographic slope. Cataclinal slopes that are steeper than the dip of the bedding plane are **overdip** slopes. Cataclinal slopes that are less steep than the dip of the bedding plane are **underdip** slopes. Cataclinal slopes that follow the bedding plane are **dip** slopes. Anaclinal slope divisions include **normal escarpments** which are perpendicular to the dip of the bedding plane, **steepened escarpments** which are steeper than the bedding plane, and **subdued escarpments** which are less steep than the bedding plane.

## 2. Methods

Calculation of a topographic/bedding-plane intersection angle at a given point requires four variables: topographic slope ( $S$ ;  $0-90^\circ$ ), slope aspect ( $A$ ;  $0-360^\circ$ ), bedding dip ( $\theta$ ;  $0-90^\circ$ ) and dip direction ( $\alpha$ ;  $0-360^\circ$ ). TOBIA can be modeled either categorically or continuously.

### 2.1. Categorical modeling

Using slope, slope aspect, dip, and dip direction, the landscape can be stratified into the slope types discussed above (Table 1). Slopes are classified into cataclinal, anacinal, and orthoclinal types based on the conformity between dip direction and slope aspect. Cataclinal slopes are classified where the difference between  $\alpha$  and  $A$  is  $0 \pm 45^\circ$ . Anaclinal slopes occur if the difference between  $\alpha$  and  $A$  is  $180 \pm 45^\circ$ , and orthoclinal slopes occur if the difference is  $90 \pm 45^\circ$  or  $270 \pm 45^\circ$ . In order to determine these differences, we compute the chord length subtended by the angle between  $\alpha$  and  $A$  on the unit circle. The chord

Table 1  
Classification of topography relative to strike and dip of bedding planes

Division	Slope type	Abbreviation	Orientation
Cataclinal	Overdip	$D_o$	$S > \theta$
Cataclinal	Underdip	$D_u$	$S < \theta$
Cataclinal	Dip	$D$	$S = \theta$
Anacinal	Steepened escarpment	$E_{st}$	$S > \theta$
Anacinal	Subdued escarpment	$E_{su}$	$S < \theta$
Anacinal	Normal escarpment	$E_n$	$S = \theta$

describes a continuous function between zero and two on the unit circle. The chord length is:

$$L = \sqrt{(\cos \alpha - \cos A)^2 + (\sin \alpha - \sin A)^2} \quad (1)$$

Each slope type is then classified based on the chord length ranges corresponding to the four categories above. These are expressed as:

$$\text{if } 0 \leq L \leq 0.7654 \quad \text{then } a_c (0^\circ \pm 45^\circ)$$

$$\text{if } 0.7654 < L \leq 1.8478 \quad \text{then } a_o (90^\circ \pm 45^\circ \text{ or } 270^\circ \pm 45^\circ)$$

$$\text{if } 1.8478 < L \leq 2 \quad \text{then } a_a (180^\circ \pm 45^\circ)$$

where  $a_c$  represents cataclinal slopes,  $a_a$  represents anaclinal slopes, and  $a_o$  represents orthoclinal slopes. Cruden and Hu (1996) note that slope types are conventionally categorized using a  $20^\circ$  range. However, the range and number of categories can be tailored to different applications. For example, a narrow range could be required for hillslope stability applications at the slope-level. However, for landscape-scale applications, such as mapping relationships between TOBIA and potential hillslope stability, substrate conditions, or vegetation patterns, the larger range is probably more appropriate given the scale and the potential error associated with spatial data. In our study area we find that topography and bedding planes are often aligned such that cataclinal and anaclinal slopes do not occur when using such a narrow range. Consequently, many locations would be mapped as orthoclinal slopes unless additional categories are used.

Cataclinal and anaclinal slopes are further partitioned based on the conformity between slope angle and dip angle. Orthoclinal slopes are not further partitioned. The following logic is used for cataclinal slopes:

$$\text{if } -5^\circ \leq \theta - S \leq 5^\circ \quad \text{then } a_c = D \text{ (dip slope)}$$

$$\text{if } \theta - S > 5^\circ \quad \text{then } a_c = D_u \text{ (underdip slope)}$$

$$\text{if } \theta - S < -5^\circ \quad \text{then } a_c = D_o \text{ (overdip slope).}$$

For anaclinal slopes:

$$\text{if } -5^\circ \leq \theta - S \leq 5^\circ \quad \text{then } a_a = E_n \text{ (normal escarpment)}$$

$$\text{if } \theta - S > 5^\circ \quad \text{then } a_a = E_{su} \text{ (subdued escarpment)}$$

$$\text{if } \theta - S < -5^\circ \quad \text{then } a_a = E_{st} \text{ (steepened escarpment).}$$

## 2.2. Continuous modeling

Topographic/bedding plane intersection angles can also be modeled in a continuous manner. To do this, we modify the logic used to model topographic variability in solar radiation (e.g. Dozier, 1980; Dubayah, 1992). An index of topographic/bedding-plane intersection angle can be expressed continuously as:

$$\text{TOBIA} = \cos \theta \cos S + \sin \theta \sin S \cos(\alpha - A). \quad (2)$$

The model calculates an index of conformity between topography and a bedding plane. Index values range from one to negative one.

We have computed a set of artificial surfaces that characterize variations in the TOBIA Index as a function only of dip angle and slope angle for cataclinal ( $\alpha - A$  is  $0^\circ$ ), anaclinal ( $\alpha - A$  is  $180^\circ$ ), and orthoclinal ( $\alpha - A$  is  $90^\circ$ ) orientations. For all three orientations, if either  $\theta$  or  $S$  are zero, then the right side of Eq. (2) reduces to zero, and the index will range from one to zero. Index values for cataclinal slopes range from one for dip slopes — where  $\theta$  and  $S$  are equivalent — to zero as  $\theta$  and  $S$  become increasingly unaligned (Fig. 2a). In the pure cataclinal case considered here, the  $\cos(\alpha - A)$  portion of the model is equal to one because  $\alpha$  and  $A$  have the same direction.

If  $\alpha$  and  $A$  are compass opposites (e.g.  $\alpha$  is  $205^\circ$  and  $A$  is  $25^\circ$ ),  $\cos(\alpha - A)$  becomes negative one and anaclinal slopes occur (Fig. 2b). In this case, TOBIA decreases if either  $\theta$  or  $S$  increase. The index ranges from almost one when  $\theta$  and  $S$  are low, through zero when they are perpendicular, to negative one when  $\theta$  and  $S$  are high. Assuming that bedding planes are dipping, index values approaching zero are associated with subdued escarpments. Values approaching negative one represent extremely steep escarpments. Intermediate between these two configurations is the normal escarpment ( $\theta$  is perpendicular to  $S$ ) which has an index value of zero.

In mountainous and hilly terrain, dip direction and slope aspect are sometimes oriented such that cataclinal and anaclinal slopes do not occur (Cruden, 1988). In these orthoclinal cases, the  $\cos(\alpha - A)$  portion of Eq. (2) adjusts index values by quantifying the degree to which dip direction and slope aspect are aligned. The product of the right side of Eq. (2) decreases as  $\alpha$  becomes increasingly perpendicular to  $A$ . Where  $\alpha$  is perpendicular to  $A$ , the right side of Eq. (2) reduces to zero. The TOBIA Index ranges from one ( $\theta$  and  $S$  are low) to zero ( $\theta$  and  $S$  are high) for orthoclinal slopes (Fig. 2c).

### 3. Application and evaluation

The models described previously are encoded and implemented in a geographic information system (GIS) in order to apply them in a spatially distributed framework. The models are applied using mapped geologic data (Dibblee, 1986) and a digital elevation model (DEM) from a small (8.2 km<sup>2</sup>) watershed (Mission Canyon) on the southern flank of the Santa Ynez Mountains, California.

Located in the Los Padres National Forest, the Santa Ynez Range forms the western portion of the Transverse Range bordering the Pacific Ocean. The lithology and geologic structure of the Santa Ynez have been described by Page et al. (1951) and mapped by Dibblee (1986; Fig. 3a). The range is mostly composed of shales and sandstones which were deposited as river and ocean sediments during the upper Eocene and Oligocene and subsequently uplifted, most rapidly during the early Pleistocene. Page et al. (1951) note that tectonic uplift oriented the strike of these beds in an east-west trending belt which is now a limb of a partially eroded anticline. The bedding planes tend to dip steeply 205° S. Dip angles range from 35° near the basin's headwaters to vertical positions (Fig. 3d). The topography is dissected into steep slopes with elevation ranging from approximately 275 m in the foothills to 1215 m at La Cumbre Peak. Many areas are capped

by resistant sandstones. The major streams typically drain away from the Santa Ynez Ridge with tributary streams usually tracking the strike of shales (e.g. Cozy Dell) that are much less resistant to weathering (Page et al., 1951).

In order to compute the spatial distribution of TOBIA across the study watershed, we derived slope and slope aspect surfaces (Figs. 3b and c) (Burrough and McDonnell, 1998) from a high resolution DEM (10 m). The DEM was developed from elevation contours digitized from USGS topographic quadrangles (1:24,000) using the TOPOGRID algorithm in Arc/Info (Hutchinson, 1989).

While DEMs are readily available, strike and dip data are usually available only in hard copy as point measurements on geologic maps. To obtain spatially distributed fields of strike and dip, we digitized 61 strike/dip points from Dibblee (1986) within and around the Mission Canyon watershed (Fig. 3a). Spatially interpolated surfaces were then produced using ordinary kriging. The strike points were adjusted 90° in order to obtain dip direction.

Kriging is frequently used to spatially interpolate point measurements in numerous Earth system science applications (e.g. Bonham-Carter, 1994; Burrough and McDonnell, 1998; Isaaks and Srivastava, 1989). Kriged estimates for some spatially distributed variable at any spatial location  $x, y$  for which the actual value of  $z$  is

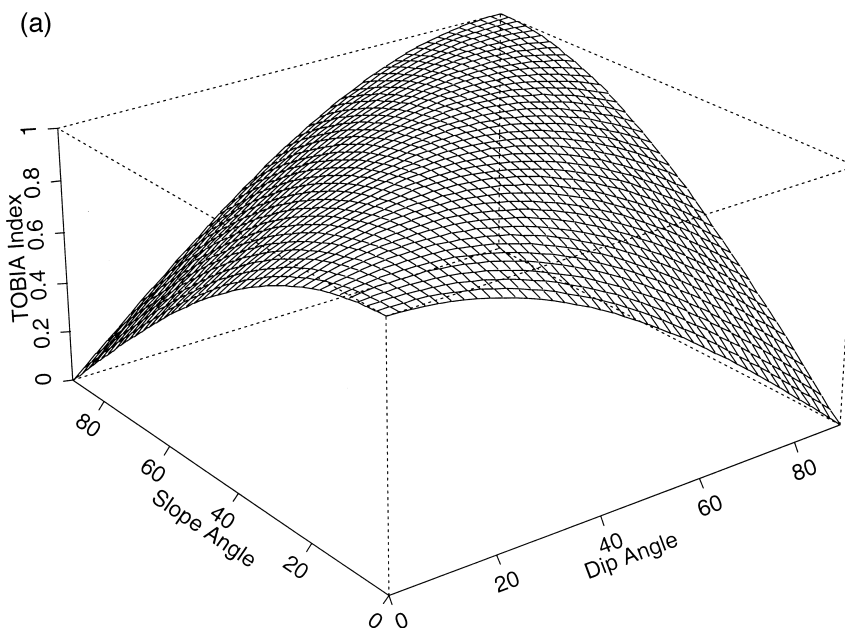


Fig. 2. (a) Artificial surface characterizing variations in continuous TOBIA Index as function only of dip angle and slope angle for pure cataclinal slopes. (b) Artificial surface characterizing variations in continuous TOBIA Index as function only of dip angle and slope angle for pure anaclinal slopes. (c) Artificial surface characterizing variations in continuous TOBIA Index as function only of dip angle and slope angle for pure orthoclinal slopes.

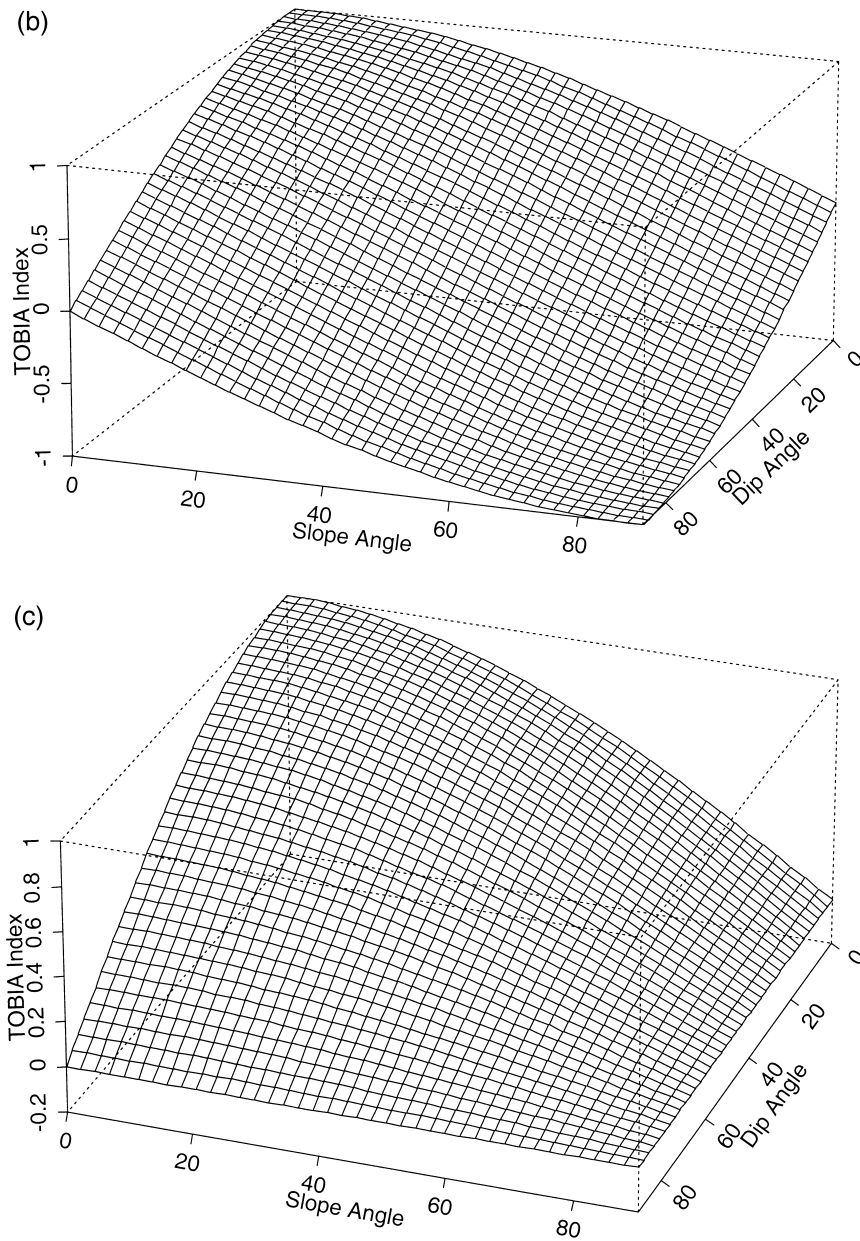


Fig. 2 (continued)

unknown, are determined via an inverse distance-weighted average of the known  $z$  values from a surrounding set of sampled points. The kriging weights are derived from a simple three-parameter model (semi-variogram) that characterizes the spatial dependence in the known data. The weights are derived such that the kriged surface will minimize the error variance, thus providing an unbiased estimate of  $z$  at any unsampled location within the spatial domain.

A primary weakness of kriging is that the fit of the

interpolation is limited by the degree to which the estimated semivariogram fits the actual semivariogram calculated from the original sampled point data. The strength of the method is that the actual spatial dependence in the phenomenon of interest is used to inform the characteristics of the inverse weighting structure. An additional advantage is the ability to determine the standard error of the estimates at any  $x, y$  location and, consequently to map the standard error surfaces. Although we use ordinary kriging, which is a global,

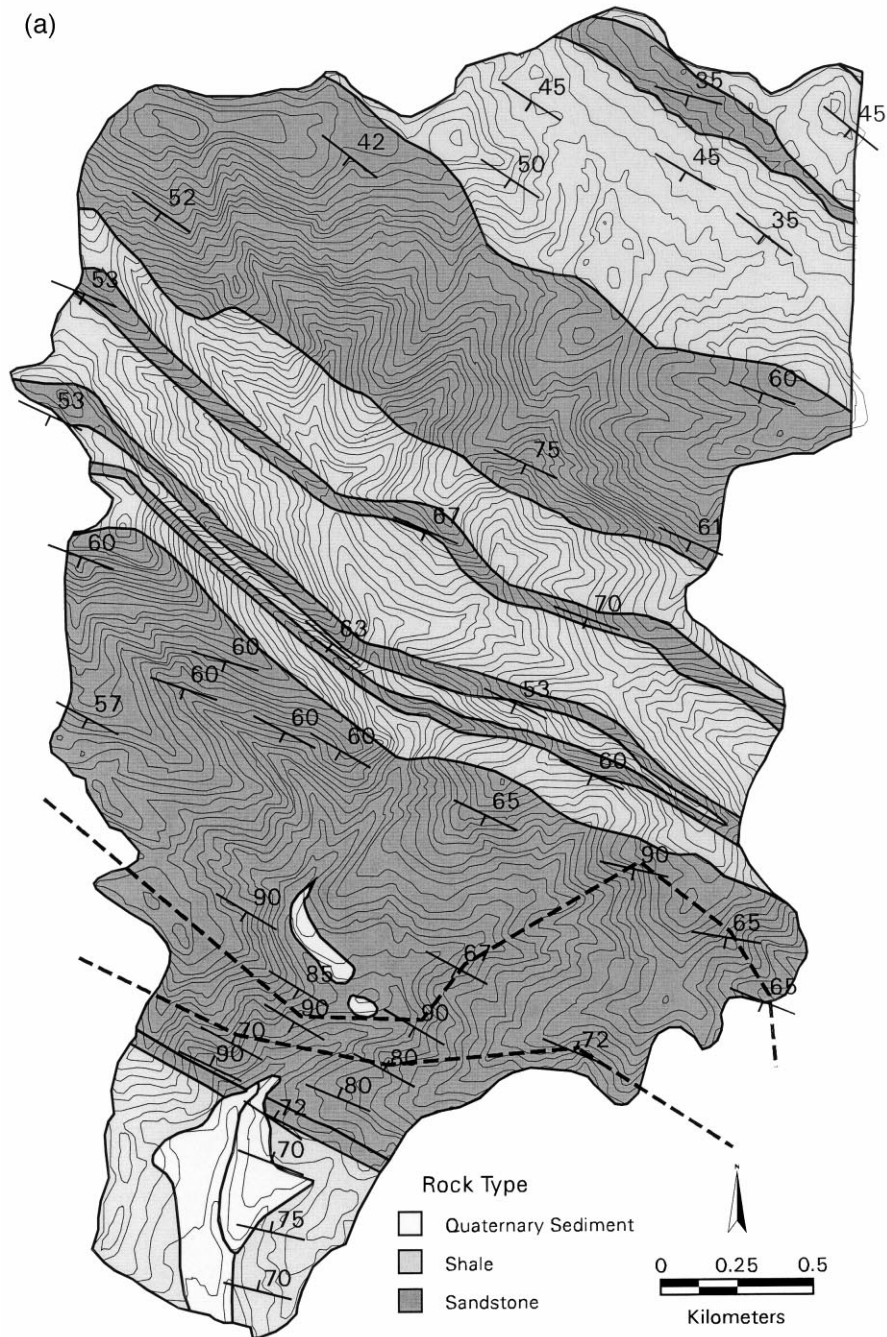


Fig. 3. (a) Digitized geologic map of Mission Canyon watershed (Dibblee, 1986). Contours represent 50 ft. elevation intervals. Symbols indicate locations of strike/dip point measurements used to spatially interpolate dip angle ( $\theta$ ; Fig. 3d) and dip direction ( $\alpha$ ) across watershed. Measurements used outside of watershed are not shown. Dashed lines indicate transition in dip direction. Upper line connects known values of south-facing bedding planes and lower line connects known values of north-facing bedding planes. Uncertainty exists in region between the lines. Center of map corresponds to approximately  $34^{\circ}30'$  latitude and  $119^{\circ}42'$  longitude. (b) Topographic slope angle ( $S$ ;  $0-90^{\circ}$ ) derived from high resolution DEM (10 m). Light tones indicate high slope values and dark tones indicate low slope values. (c) Topographic slope-aspect ( $A$ ;  $0-360^{\circ}$ ) derived from high resolution DEM (10 m). Light tones indicate high slope-aspect values and dark tones indicate low slope-aspect values. (d) Spatially interpolated surface (via ordinary kriging) of dip angle ( $\theta$ ;  $0-90^{\circ}$ ). Kriging weights were derived using spherical semivariogram model. Range, sill, and nugget of estimated semi-variogram model for interpolated dip surface are 1570, 119, and 0 m, respectively. (e) Map of standard error from dip interpolation. Dark and light areas indicate high and low degree of confidence, respectively.

(b)



Fig. 3 (continued)

(c)

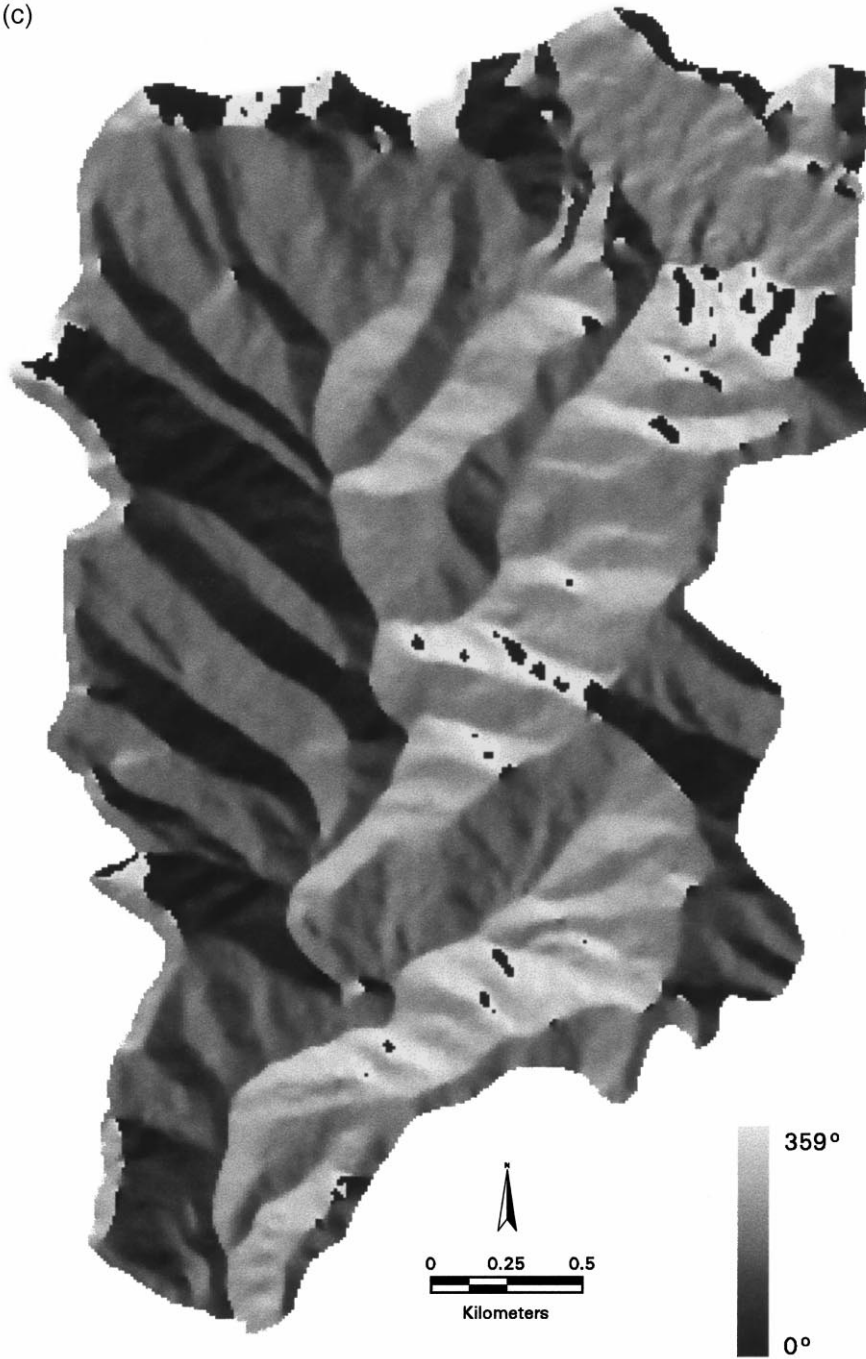


Fig. 3 (continued)

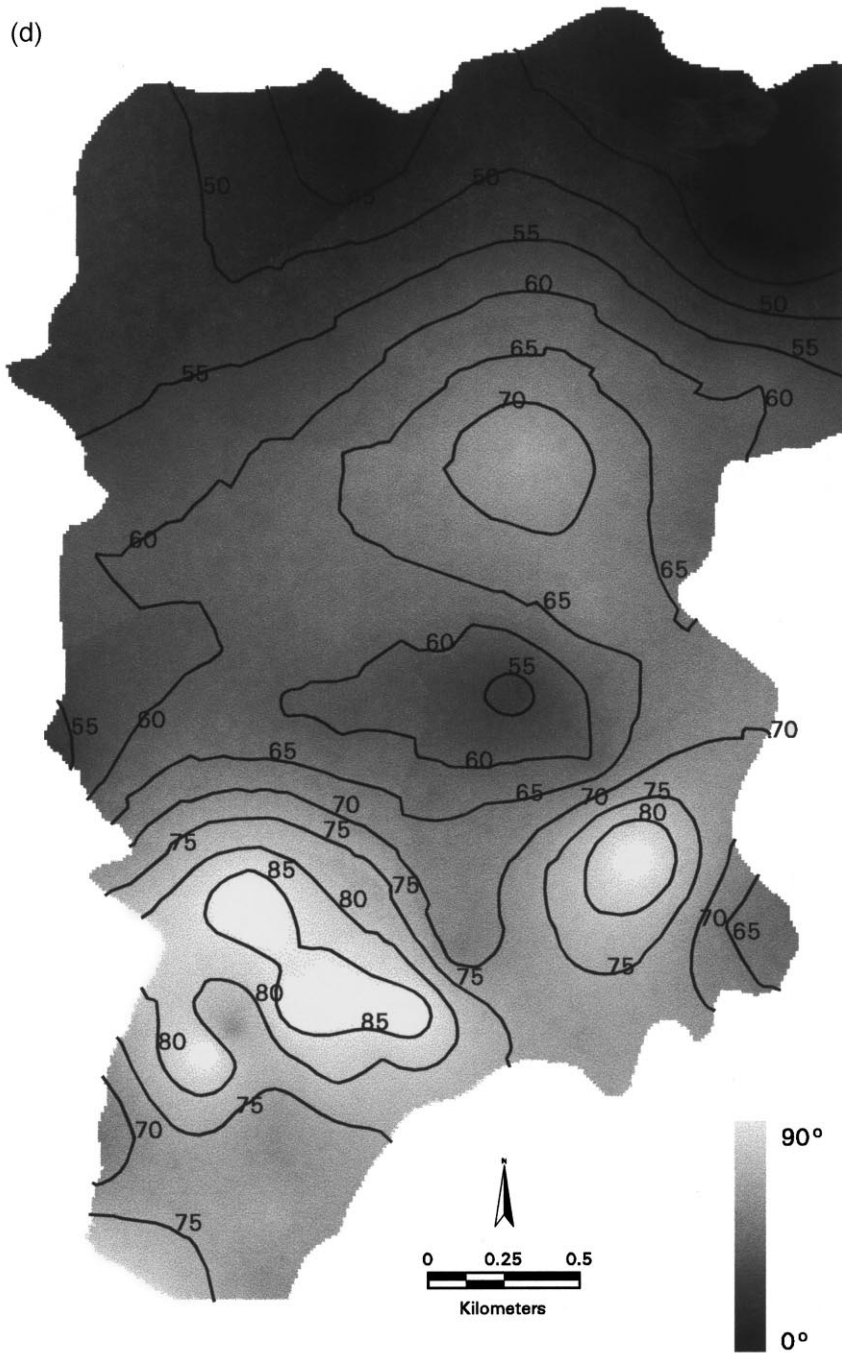


Fig. 3 (continued)

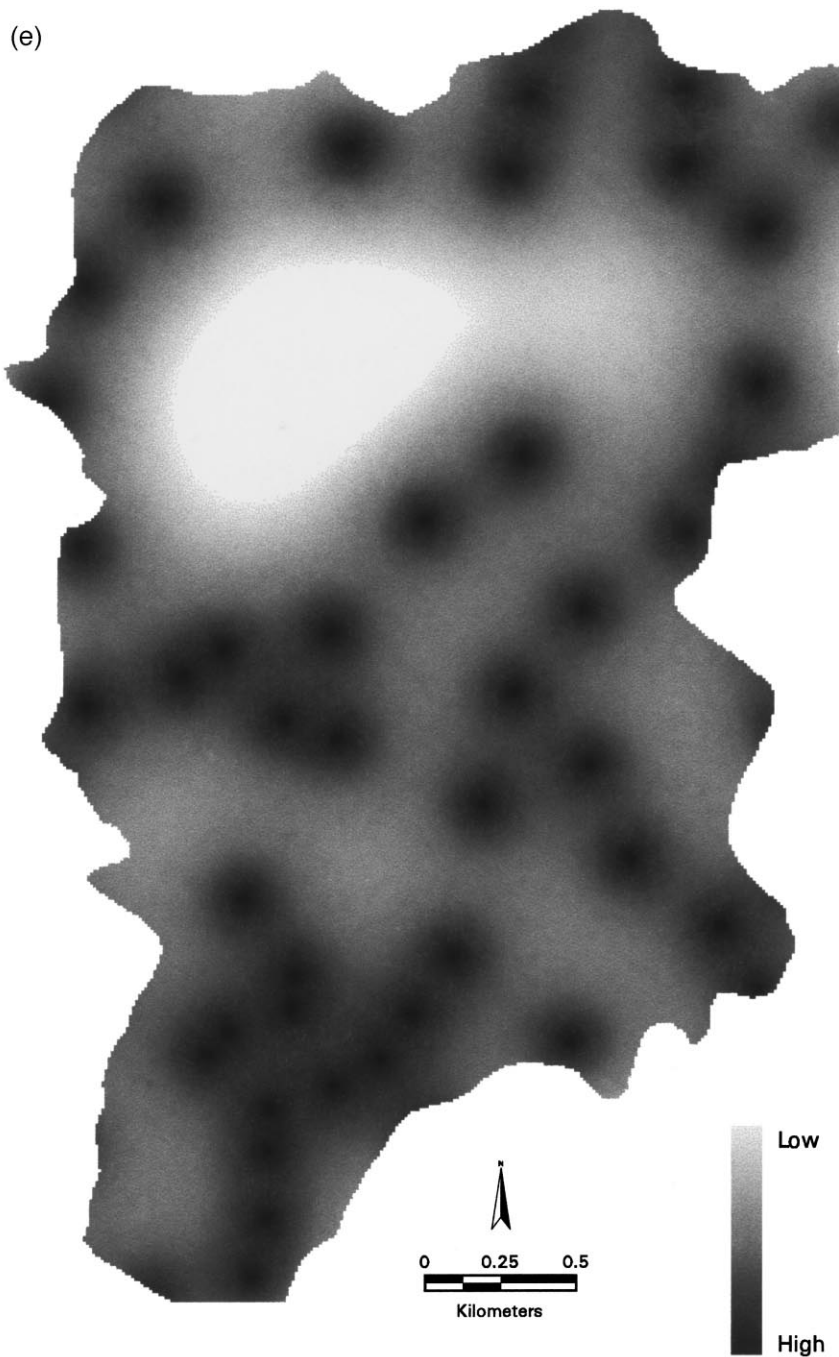


Fig. 3 (continued)

stochastic interpolator, there are numerous variations on this basic method that are often used. Discussions of the family of kriging approaches can be found in Bonham-Carter (1994), Burrough and McDonnell (1998), and Isaaks and Srivastava (1989).

Ordinary kriging was used to spatially interpolate dip (Fig. 3d) and dip direction surfaces from the digitized points. The range, sill, and nugget of the estimated semi-variogram model used to produce kriging weights for the interpolated dip surface are 1570, 119 and 0 m, respectively. The range indicates the distance over which bedding dip is spatially autocorrelated. At a distance of 1570 m, the semi-variance asymptotes around some maximum value, the sill. The nugget value represents the spatially uncorrelated noise and is low because the sample spacing is relatively small (10 m). The range, sill, and nugget of the estimated semi-variogram model for dip direction are 1360, 121 and 1.6 m.

Fig. 3e is a map of standard error from the dip interpolation. Kriged surfaces are unstable (i.e. have a high standard error) near the spatial extremes of the original data points or where sampling density is low (Fig. 3e). Strike/dip points were included from beyond the boundaries of the study area in order to produce reliable estimates at the periphery.

Other errors can occur when interpolating dip direction directly due to the occurrence of numerical gaps in crossing over Cartesian quadrant boundaries (de Kemp, 1998). For example, directly interpolating between two directional values of 10 and 350° could produce an erroneous value of 170° rather than a value closer to 0 or 360°. Alternatively, geologic structure can be decomposed into direction cosines to avoid this interpolation problem (see de Kemp, 1998). This is not such a problem in this study area because the bedding structure is relatively simple; the majority of the beds dip in a south-southwest direction. However, at the base of the watershed, a few of Dibblee's (1986) point measurements dip in a northern direction. The boundary that separates the general south-facing and overturned north-facing beds is not explicitly indicated on the Dibblee map (1986). Lines connecting the known values of the south-facing and locally overturned beds are shown in Fig. 3a. The region of uncertainty exists between the lines. Rather than subjectively inserting a barrier within this region, we have allowed the kriging model to represent the transition. The kriged dip azimuth surface undoubtedly contains a degree of error between the known points. Although none exist at this site, major faults can also introduce error and should, therefore, be treated as barriers when interpolating in order to preserve abrupt transitions in bedding structure.

Using the derived surfaces of slope, slope aspect, bedding dip, and dip direction, the categorical and

continuous TOBIA models are applied across the watershed. Figs. 4 and 5 illustrate spatially distributed estimates of topographic-bedrock intersection angles calculated using the categorical and continuous models, respectively.

The categorical map (Fig. 4) illustrates logical variations in slope types as a function of different slope, slope aspect, dip, and dip direction combinations. Most cataclinal slopes correspond to south-facing terrain. Point *A* on Fig. 4 depicts a cataclinal underdip slope. Note that the topographic slope is generally south-facing and has a relatively shallow gradient. Underdip slopes also correspond to south-facing drainages and ridges as they are typically less steep. Overdip slopes typically occur along steep, south-facing hillslopes (Point *B*). Field observations indicate that the mapped overdip slopes often correspond to the most resistant and frequently exposed sandstone formations. Dip slopes typically occur where there are moderately inclined hillslopes in this watershed (Point *C*). The lower presence of dip slopes is probably due to the narrower criteria for their classification (10°). These relationships are consistent across the watershed except where dip azimuth reverses directions (Fig. 3a) in the lower portion of the watershed.

Anaclinal slopes are typically associated with north-facing slopes (Fig. 4). Similar to the cataclinal scenarios, steepened escarpments are associated with steep, north-facing slopes (Point *D*), subdued escarpments correspond to shallow slopes (Point *E*), and normal escarpments occur along moderately inclined slopes (Point *F*). Although most of the anaclinal orientations in this watershed correspond to north-facing slopes, the escarpment at Point *E* is associated with a south-facing slope because of the switch in dip direction just above it (Fig. 3a).

Orthoclinal slopes compose the largest percent of map area (41%) in the watershed (Table 2). This is not surprising given that the orthoclinal range is twice as large as the cataclinal and anaclinal ranges, and it is not further subdivided. Due to the east–west trending strike of the bedding planes, orthoclinal slopes are typically distributed on east- and west-facing slopes (Point *G*). Underdip slopes and overdip slopes both constitute the same portion of the watershed (15%), followed by dip slopes (11%). Subdued, and normal, steepened escarpments constitute 8, 6, and 3.2% of map area, respectively. The lower occurrence of anaclinal slopes is expected given that the study site is positioned on the south flank of the mountain range and the dip azimuth is generally south-facing as well.

The application of the continuous TOBIA Index across the watershed (Fig. 5) produces the same general patterns as the categorical TOBIA map. High index values (e.g. >0.68) correspond to cataclinal slopes, and low index values (e.g. <−0.44) correspond

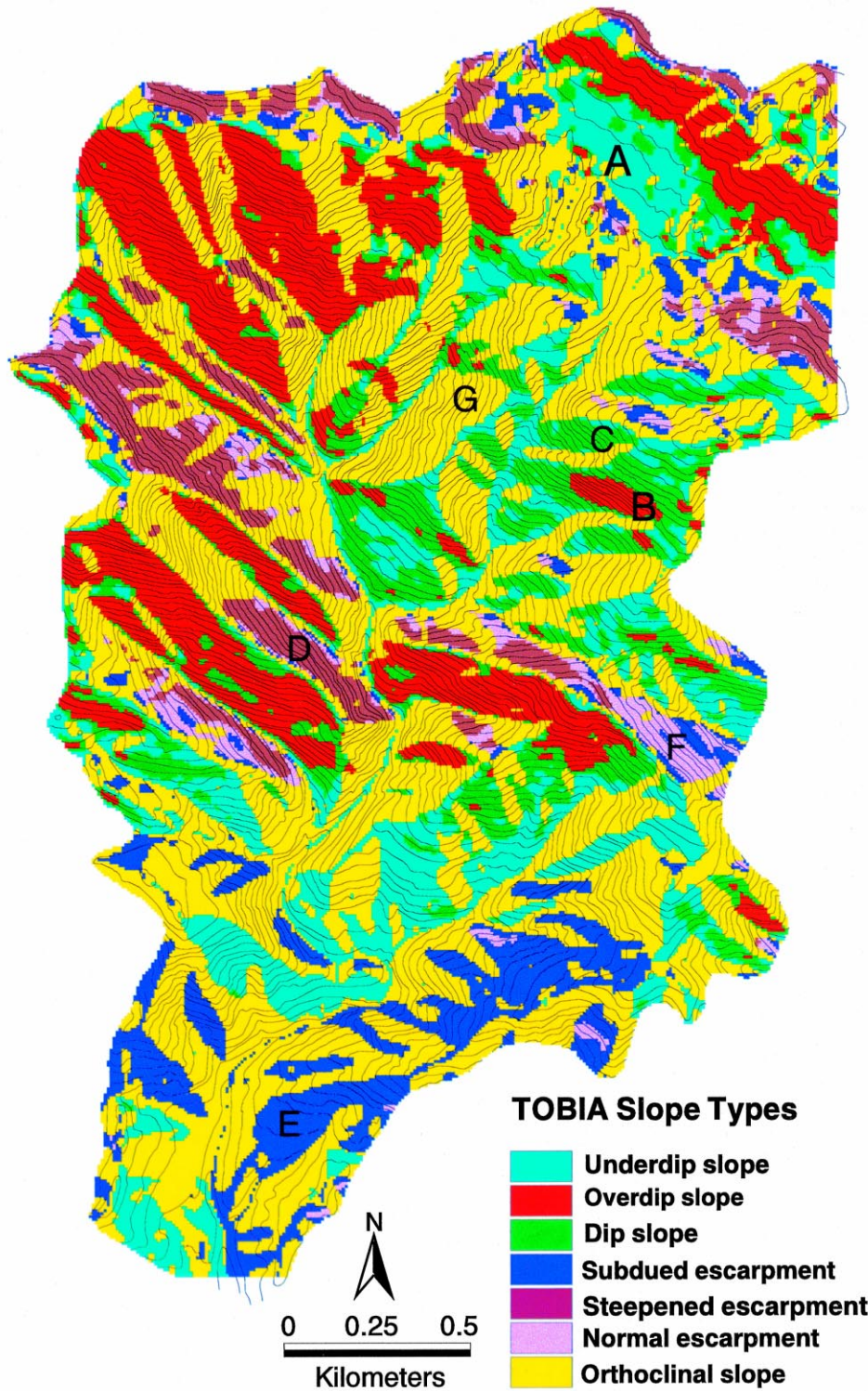


Fig. 4. Spatially distributed estimates of topographic-bedrock intersection angles using categorical model. Slope types include: underdip slopes (Point *A*), overdip slopes (Point *B*), dip slopes (Point *C*), steepened escarpment (Point *D*), subdued escarpments (Point *E*), normal escarpments (Point *F*), and orthoclinal slopes (Point *G*). See Fig. 1 for visualization of geometric relationships.

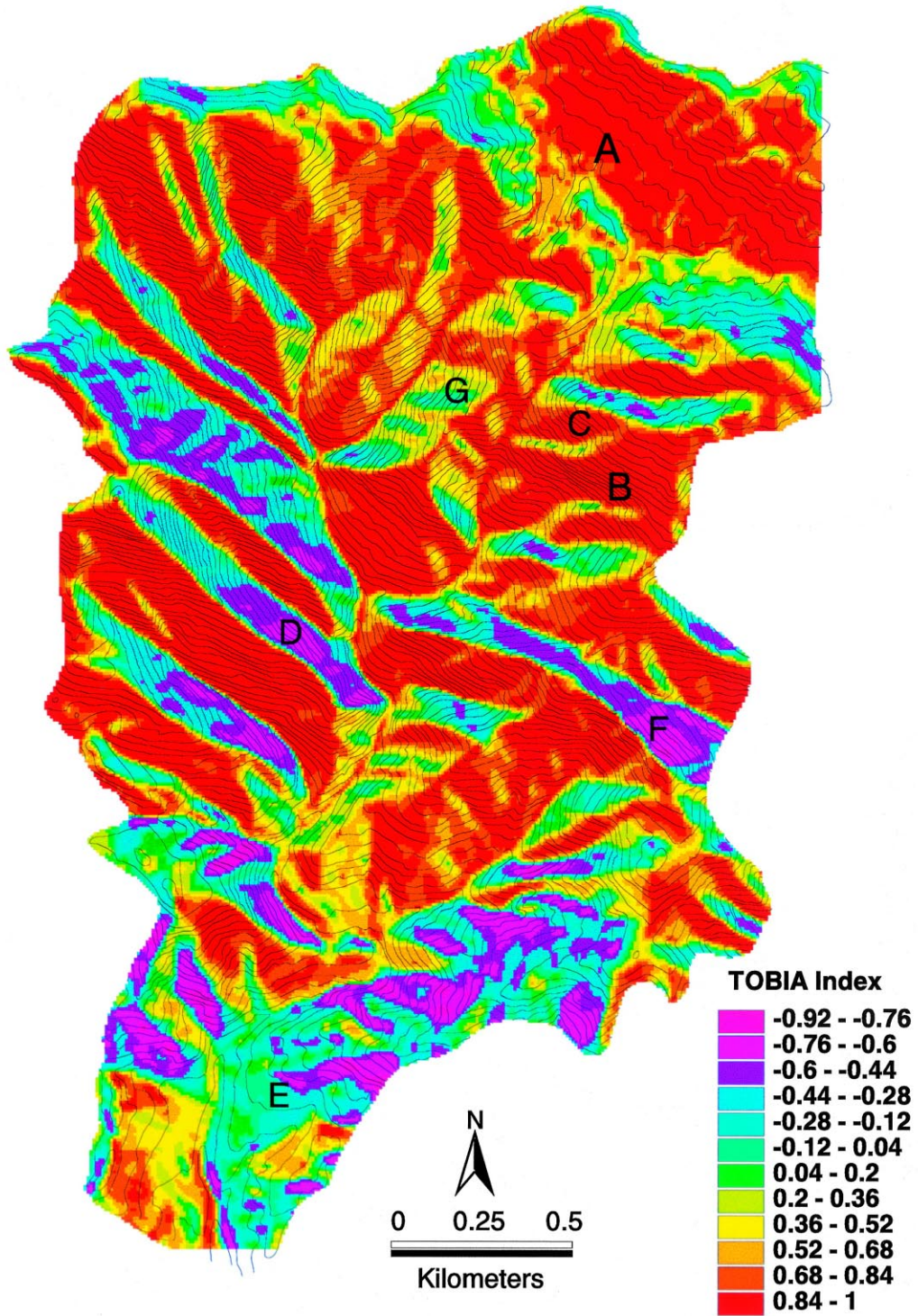


Fig. 5. Spatially distributed estimates of topographic-bedrock intersection angles using continuous model. Index values range from one to negative one. High values indicate conformity between slope, slope-aspect, dip, and dip aspect. Low values indicate unaligned orientations.

to anaclinal slopes. As expected, the highest TOBIA Index values correspond with areas that the categorical model maps as dip slopes. Conversely, the lowest index values correspond with escarpments. Moderate index values generally correspond to east- and west-facing orthoclinal slopes. Additionally, index values of ridges and drainages are often intermediate between dip slopes and escarpments as they represent a transition in slope and slope aspect.

An advantage of the continuous representation over the categorical representation is that it permits greater detail in mapping transitions of topographic/bedding plane intersection angles. A disadvantage of the continuous representation, however, is that the model does not produce unique outputs. For example, the index does not indicate if a cataclinal slope with a high index value is slightly underdip or overdip, but just that the slope and slope aspect are closely aligned with the dip and dip aspect. However, the categorical slope type is also known at any location on the continuous TOBIA Index map. By overlaying both outputs, the conformity between topography and bedding planes can be continuously represented within each of the categorically mapped slope types.

Two- and 2.5-dimensional GIS-based modeling methods can provide valuable distributed data, however, resulting cartographic representations can be difficult for a user to envision three-dimensional geometric relationships (de Kemp, 1998). Tools for better depth visualization and complete three-dimensional landscape modeling, however, can be developed (e.g. de Kemp, 1999). Future work should also focus on three-dimensional visualization of geometric relationships between topography and geological surfaces.

Although the models work well in this application, the test watershed has relatively simple structure relative to some other mountain ranges. In a structurally complex area, the methods presented may not work as

well due to error associated with spatially interpolating dip and dip direction. Regardless of the structural complexity, however, interpolation of structure will introduce error in the spatial estimation of TOBIA, and error may increase as the density of strike/dip measurements decreases. For many areas, the relatively high density of strike/dip measurements used in this application are not available. However, these data may be derived by other means. For example, using a DEM and a three-point method, Chorowicz et al. (1991) computed strike and dip at the crossing points between geological contacts and thalweg landforms. de Kemp (1999) has also provided a useful program (“trace.awk”) to calculate geologic structure automatically with DEM intersections and Morris (1991) produced strike and dip using a DEM in combination with remote sensing techniques.

#### 4. Conclusion

Digital elevation models and digitized geologic structure data are used to automatically map the alignment between topography and the orientation of bedding planes. Computation of the spatial distribution of TOBIA requires the derivation of four surfaces: topographic slope, slope aspect, bedding dip, and dip azimuth. TOBIA can be digitally mapped categorically as slope types, continuously, or by overlaying both outputs. The methods provide an efficient means for estimating topographic/bedding-plane intersection angles over large areas. Application of the categorical and continuous models across the study watershed illustrate logical transitions in slope types and degrees of conformity between topography and bedding planes. These surfaces are useful for a variety of landscape-scale modeling applications, such as the prediction of potential hillslope failure, hydrologic flow paths, substrate conditions, and vegetation patterns. Future work should focus on extending 2.5-dimensional GIS-based modeling to complete three-dimensional landscape modeling for better visualization of geometric relationships between topography and geological surfaces.

Table 2  
Percent map area of each slope type as computed by categorical TOBIA model. Slope types correspond to Fig. 4

Division/slope type	Map area (%)
Cataclinal	
Overdip	15.4
Underdip	15.1
Dip	11.2
Anaclinal	
Steepened escarpment	3.2
Subdued escarpment	8.1
Normal escarpment	6.0
Orthoclinal	41.1

#### Acknowledgements

The authors gratefully acknowledge Larry Band, Søren Brun and Dionne Gesink-Law for generous input. This research is partially supported under NASA grant NAG5-6583.

#### References

Bonham-Carter, G.F., 1994. Geographic Information Systems

- for Geoscientists: Modelling with GIS. Pergamon, Oxford, 398 pp.
- Burrough, P.A., McDonnell, R.A., 1998. Principles of Geographical Information Systems. Oxford University Press, Oxford, 333 pp.
- Chorowicz, J., Breard, J.Y., Guillaude, R., Morasse, C.R., Prudon, D., Rudant, J.P., 1991. Dip and strike measured systematically on digitized three-dimensional geological maps. *Photogrammetric Engineering and Remote Sensing* 57 (4), 431–436.
- Chorowicz, J., Parrot, J.F., Taud, H., Hakdaoui, H., Rudant, J.P., Rouis, T., 1995. Automated pattern-recognition of geomorphic features from DEMs and satellite images. *Zeitschrift fur Geomorphologie* 101, 69–84.
- Cruden, D.M., 1988. Thresholds for catastrophic instabilities in sedimentary rock slopes. *Zeitschrift fur Geomorphologie* 67, 67–76.
- Cruden, D.M., 1989. Limits to common toppling. *Canadian Geotechnical Journal* 27, 737–742.
- Cruden, D.M., Hu, X.Q., 1996. Hazardous modes of rock slope movement in the Canadian Rockies. *Environmental and Engineering Geoscience* 2 (4), 507–516.
- de Kemp, E.A., 1998. Three-dimensional projection of curvilinear geological features through direction cosine interpolation of structural field observations. *Computers & Geosciences* 24 (3), 269–284.
- de Kemp, E.A., 1999. Visualization of complex geological structures using 3-D Bezier construction tools. *Computers & Geosciences* 25 (5), 581.
- Dibblee, T.W., 1986. Geologic Map of the Santa Barbara Quadrangle. Published by Thomas Dibblee Jr, Geological Foundation.
- Dozier, J., 1980. A clear-sky spectral solar radiation model for snow-covered mountainous terrain. *Water Resources Research* 16, 709–718.
- Dubayah, R.C., 1992. Estimating net solar radiation using Landsat Thematic Mapper and digital elevation data. *Water Resources Research* 28, 2469–2484.
- Eaton, T.M., 1986. Reconnaissance of rockslide hazards in Kananaski Country. M.Sc. thesis, University of Alberta, Edmonton, 291 pp.
- Freeze, R.A., Cherry, J.A., 1979. *Groundwater*. Prentice-Hall, Englewood Cliffs, NJ, 604 pp.
- Hutchinson, M.F., 1989. A new procedure for gridding elevation and streamline data with automatic removal of spurious pits. *Journal of Hydrology* 106, 211–232.
- Ichoku, C., Chorowicz, J., Parrot, J.F., 1994. Computerized construction of geological cross sections from digital maps. *Computers & Geosciences* 20 (9), 1321–1327.
- Isaaks, E.H., Srivastava, R.M., 1989. *An Introduction to Applied Geostatistics*. Oxford University Press, Oxford, 561 pp.
- Morris, K., 1991. Using knowledge-based rules to map the three-dimensional nature of geological features. *Photogrammetric Engineering and Remote Sensing* 57 (9), 1209–1216.
- Page, B.M., Marks, J.G., Walker, G.W., 1951. Stratigraphy and structure of mountains northeast of Santa Barbara, California. *Bulletin of the American Association of Petroleum Geologists* 15 (8), 1727–1780.
- Powell, J.W., 1875. *Exploration of the Colorado River of the West and its Tributaries*. Government Printing Office, Washington, DC 291 pp.
- Sander, B., 1970. *An Introduction to the Study of the Fabric of the Geological Bodies*. Pergamon, Oxford 641 pp.
- Selby, M.J., 1993. *Hillslope Materials and Processes*. Oxford University Press, Oxford 451 pp.